Korean J. Chem. Eng., 39(8), 2182-2191 (2022)
DOI: 10.1007/s11814-022-1065-8

pISSN: 0256-1115
eISSN: 1975-7220

Thermal and electrical conductivity improvement in epoxy resin with expanded graphite and silver plating

Fan-Long Jin*,†, Na Chu*,, Shan-Shan Yao*, and Soo-Jin Park***,†**

*Department of Polymer Materials, Jilin Institute of Chemical Technology, Jilin City 132022, P. R. China
**College of Chemistry, Jilin University, Changchun City 130012, P. R. China
***Department of Chemistry, Inha University, Michuhol-gu, Incheon 22212, Korea
(*Received 30 October 2021 • Revised 25 December 2021 • Accepted 13 January 2022*)

Abstract−To improve the thermal and electrical conductivity of diglycidylether of bisphenol-A (DGEBA), expanded graphite (EG) was added to the DGEBA matrix and the EG surface was silver plated. The effect of EG content on the thermal and electrical conductivity, thermal property, flexural properties, impact strength, and morphology of the DGEBA/EG composites was investigated. The silver plating on the EG surface was confirmed via high-resolution scanning electron microscopy, energy-dispersive X-ray spectrometry, and X-ray photoelectron spectroscopy. The results indicate that the thermal conductivity of the DGEBA/EG composites containing 60 wt% of EG was 7.35 W/m·K, which was 42 times higher than that of the pristine DGEBA. In addition, the thermal conductivity of the DGEBA/EG composites further increased from 7.35 to 9.49 W/m·K after the EG surface was silver plated. The electrical conductivity of the DGEBA/EG composites increased from 0 to 0.62 S/cm with the addition of 60 wt% of EG and further increased to 0.78 S/cm after silver plating of the EG surface.

Keywords: DGEBA, Expanded Graphite, Silver Plating, Thermal Conductivity, Electrical Conductivity

INTRODUCTION

Epoxy resins contain two or more epoxy groups that can be cross-linked into a three-dimensional network under certain curing conditions. They exhibit excellent thermal stability, high electrical insulation performance, low shrinkage, strong reactivity, and feature active and controllable functional groups [1,2]. Different types of epoxy resins, reaction modes, and linking structures can be designed to meet different performance and application requirements. Consequently, epoxy resins are widely used in coatings, adhesives, sealing materials, plate forming, and as matrices for composites [3,4].

The rapid evolution of the semiconductor and energy storage technologies has resulted in the development of advanced devices with high integration density and high-power requirement. As a result, there is a growing demand for materials that can satisfy the heat dissipation requirements of such highly integrated and high-power devices. Therefore, the preparation of high-heat conducting materials has become a hot topic in scientific research [5]. Although epoxy resins are well-known thermosetting resins owing to their excellent chemical and solvent resistance, their low thermal conductivity limits their application as heat conducting materials [6].

The thermal conductivity of a material mainly depends on the vibration of phonons, photons, and electrons. Preparation methods of heat conducting materials usually include intrinsic and filler modifications. Most epoxy-based polymers possess large relative molecular weights, and their molecular weights and molecular sizes exhibit polydispersity. The molecular chain existing in random line groups with an uneven structure is difficult to crystallize completely, causing the poor thermal conductivity of epoxy-based polymers. Therefore, a special physical structure such as chain regularity and long-range ordered structures can be obtained by optimizing the group structure of the epoxy resins and the molecular chain structure of the cured epoxy resins. Such structural optimizations cause the material to exhibit high phonon and electron transmission. However, this method has several disadvantages, such as the requirements of stringent experimental environments and reaction conditions, as well as impedes the mass production of such materials. In contrast, filler modification is the most feasible and low cost method that aids the large-scale industrialization of epoxy-based devices [7-10].

The types of fillers used in the preparation of heat-conducting materials include metals, carbon-based materials, and inorganic particles. Metals such as gold, silver, copper, iron, and aluminum are usually preferred as metal-based fillers [11]. In contrast, carbon-based materials such as graphene, carbon fiber, carbon nanotubes, and graphite, which exhibit good thermal and electrical conductivities as well as a high mechanical strength, are used as typical carbon-based fillers [12]. Inorganic particles include diatomic substances, such as silicon nitride, silicon carbide, and boron nitride. By selecting the type and size of the inorganic fillers, the thermal conductivity of the heat conducting materials can be improved. Moreover, the thermal conductivity and mechanical properties can be optimized via surface treatment of the fillers [13].

Among these fillers, expanded graphite (EG) is a type of filler material with a loose porous structure that is obtained via the processing of natural graphite, which is inexpensive and easily avail-

†To whom correspondence should be addressed.
E-mail: jinfanlong@163.com, sjpark@inha.ac.kr

able. The EG contains numerous loose mesh holes on its surface and inside, possesses a large specific surface area, and exhibits good adsorption capacity. Owing to these advantageous characteristics, EG has been widely used in recent years [14-16]. In general, the EG surface is treated using silane coupling agents, ozone, ionic liquid, and silver. Among the commonly used metals, silver exhibits the best thermal conductivity, good chemical operability, and is relatively safe to use. Silver plating includes the calcination, mixing, and solution methods [17,18], among which, the solution method has the following advantages: First, an alkaline solution slightly modifies the EG surface; second, the large number of holes and gaps in the interior of the EG can accommodate a large amount of silver after the silver plating; thus, a large contact area between the EG and the polymer matrix can be developed, resulting in a high thermal conductivity [19,20].

Thus, this study was performed to develop a feasible method to improve the thermal and electrical conductivity of an epoxy resin. In this study, diglycidylether of bisphenol-A (DGEBA)/EG composites, with and without silver plating, were prepared via melt blending and compression-curing processes. The effect of EG content on the thermal and electrical conductivities, thermal properties, flexural properties, impact strength, and morphology of the DGEBA/EG composites was investigated.

EXPERIMENTAL

1. Materials

The DGEBA with an epoxy equivalent weight of 184-195 g/mol was supplied by Nantong Xingchen Synthetic Material Co., Ltd. EG with a particle size of 40 meshes, carbon content of 98-99%, expansion rate of 100-400, and thermal conductivity of 300 W/m·K was obtained from Jiangxi Shuobang New Material Technology Co., Ltd. Anhydrous ethanol, acetic acid, silver nitrate solution, and 25 wt% glucose solution were supplied by Sinopharm Chemical Resilverent Co. Ltd., Fuchen Chemical Resilverent Co., Ltd., Guangzhou Hewei Pharmaceutical Technology Co., Ltd., and Heilongjiang Qitai Animal Health Products Co. Ltd., respectively. Sodium hydroxide and ammonia solutions were obtained from Tianjin Damao Chemical Resilverent Factory. All the chemicals were of analytical grade and were used without further purification.

2. Synthesis of BPH

Pyrazine (2.4 g, 0.05 mol), benzyl bromide (6.16 g, 0.036 mol), and acetonitrile (15 mL) were added into a 250 mL conical flask, and the mixture was stirred and left to react at room temperature for four days. After the reaction was complete, the precipitated solid was collected via filtration and washed with methanol and ether. The solid product was dried in vacuum and added to a solution of $NaSbF_6$ in H_2O, and the mixture was stirred for 30 min. The anion-exchange product was filtered, washed with ether, and then dried in vacuum. The resulting product was re-crystallized from methanol, and 77% white crystals were obtained.

3. Silver Plating of EG

The preparation of the Ag@EG is schematically illustrated in Fig. 1 and the details are as follows. Preparation of silver ammonia solution: Initially, 0.1 mol/L silver nitrate solution (60 mL) was diluted with deionized water (200 mL) via constant stirring. Next, 0.1 mol/L sodium hydroxide solution (60 mL) was added dropwise to the silver nitrate solution until precipitation was complete. Then, 0.1 mol/L ammonia solution (120 ml) was added to the solution until the precipitation disappeared completely.

Silver plating of EG: EG (40 g) was added to the silver ammonia solution at 65 °C and stirred for 30 min. Next, 25 wt% glucose solution (5 mL) was added to the EG mixture, and the mixture was heated to 65 °C and maintained at this temperature for 1 h. The mixture was vacuum-filtered, washed to neutrality, dried at 80 °C for 3 h, and ground to obtain silver-plated EG (for convenience,

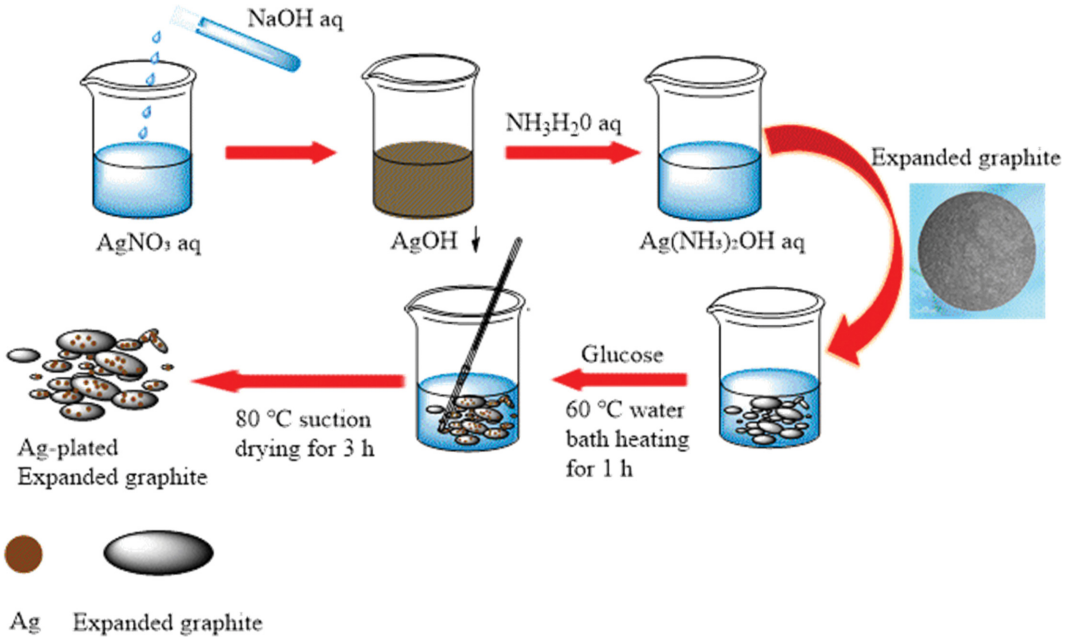

Fig. 1. Schematic illustration of the synthetic procedures of Ag@EG.

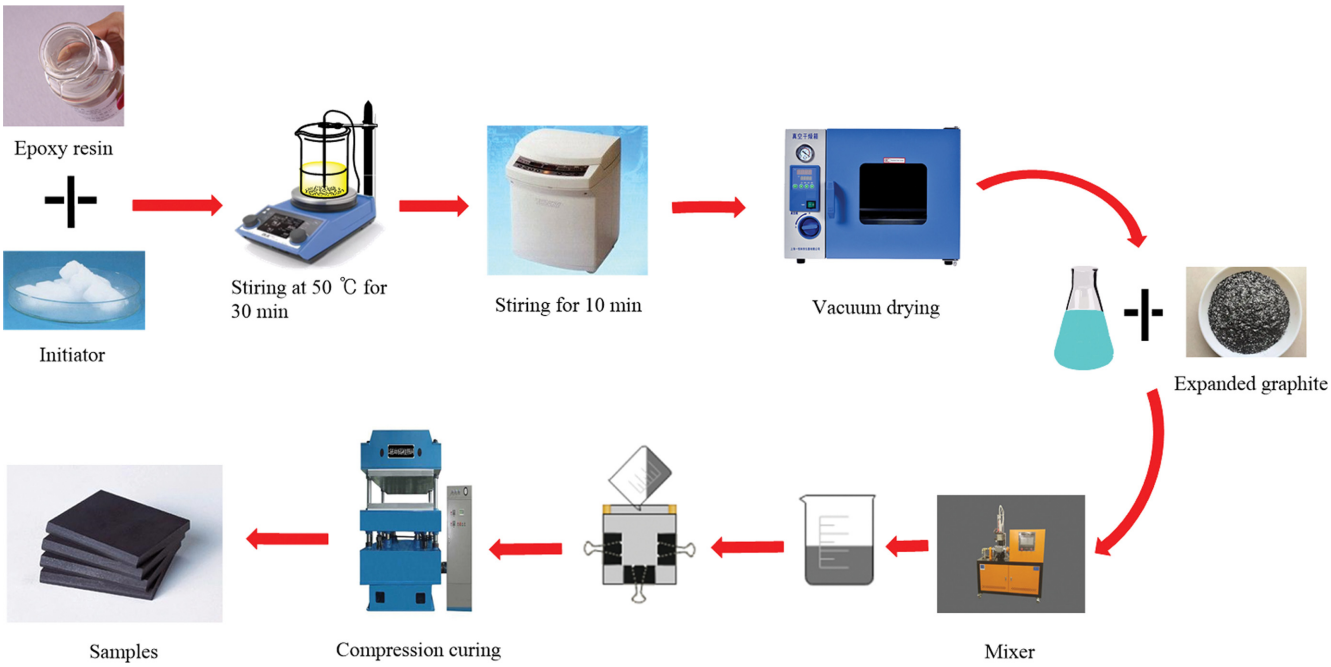

Fig. 2. Schematic illustration of the preparation of DGEBA/EG and DGEBA/Ag@EG composites.

the silver-plated EG is denoted as Ag@EG in this paper).

4. Preparation of the DGEBA/EG and DGEBA/Ag@EG Composites

The preparation of the DGEBA/EG and DGEBA/Ag@EG composites is schematically shown in Fig. 2. The desired amounts of DGEBA, EG/Ag@EG, and BPH were mixed in a mixer at 80 °C for 30 min. Then, the mixture was injected into a preheated mold sprayed with a mold release agent. The mold was compression-cured at 130, 180, and 220 °C under a pressure of 5 MPa for 1 h. The specimens were cut to suitable dimensions for the subsequent thermal and mechanical tests.

5. Characterization and Measurements

The Fourier-transform infrared (FTIR) spectra of EG and Ag@EG were obtained using an FT-IR spectrometer (Tensor II, Bruker Company, Germany) with KBr pellets. The surface morphology of EG and Ag@EG was investigated via high-resolution scanning electron microscopy (HR-SEM; Hitachi, SU 8010). Energy-dispersive X-ray spectroscopy (EDX) and SEM were performed to evaluate the presence of silver on the EG surface. The surface properties of EG and Ag@EG were evaluated using X-ray photoelectron spectroscopy (XPS; Thermo ESCALAB 250) with a monochromatic Al Kα source and a passing energy of 20 eV.

The thermal conductivity of the synthesized DGBA/EG composites was measured using a thermal conductivity tester (WNK-100) following the GB/T 10294-2008 standard. This test was conducted using samples each of size 5×10×30 mm^3. The thermal conductivity values were obtained by taking the average of three experimental values.

The resistivity of the composites was measured at room temperature using a DC resistance tester (ZC-90) according to the GB/T 24525-2009 standard. This test was performed using samples each of size 4×80×80 mm^3. The electrical conductivity (σ) was calculated using the following equation:

$$\sigma = \frac{L}{RS} \quad (1)$$

where L is the sample thickness, R is the measured resistivity, and S is the cross-sectional area of the sample. The electrical conductivity values were also obtained by taking the average of three experimental values.

The thermal stability of the composites was evaluated via thermogravimetric analysis (TGA; TA Instruments, Q50) between 30 and 800 °C at a scanning rate of 10 °C/min under nitrogen atmosphere.

The flexural property of the composites was investigated via a three-point bending test using a mechanical testing apparatus (WDW

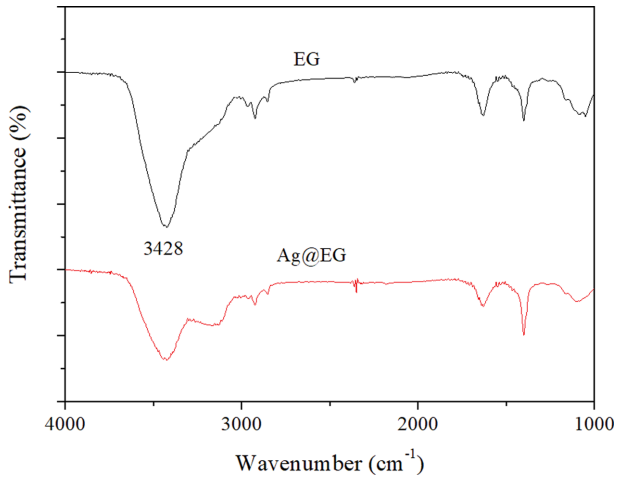

Fig. 3. FTIR spectra of EG and Ag@EG.

3010) according to the GB/T 9341-2008 standard. The sample size for this test was 4×10×80 mm^3, and the cross-head speed was kept 2 mm/min. The flexural strength (σ_f) and elastic modulus (E_b) values were calculated using the following equations:

$$\sigma_f = \frac{3PL}{2bd^2} \quad (2)$$

$$E_b = \frac{L^3}{4bd^3}\frac{\Delta P}{\Delta m} \quad (3)$$

where P is the applied load (in N), L is the span length (in mm), b is the width of the specimen (in mm), d is the thickness of the specimen (in mm), ΔP is the change in force in the linear portion of the load-deflection curve (in N), and Δm is the corresponding change in deflection (in mm). The flexural strength and modulus values were obtained by taking the average of five experimental values.

The impact strength of the composites was measured using an Izod impact tester (TP04G-AS1) according to the GB/T 1843-2008 standard. The sample size for this test was 4×10×50 mm^3. The impact strength values were obtained by taking the average of five experimental values.

The morphology of the pristine DGEBA and the DGEBA/EG composites was examined using SEM (Hitachi, S4800).

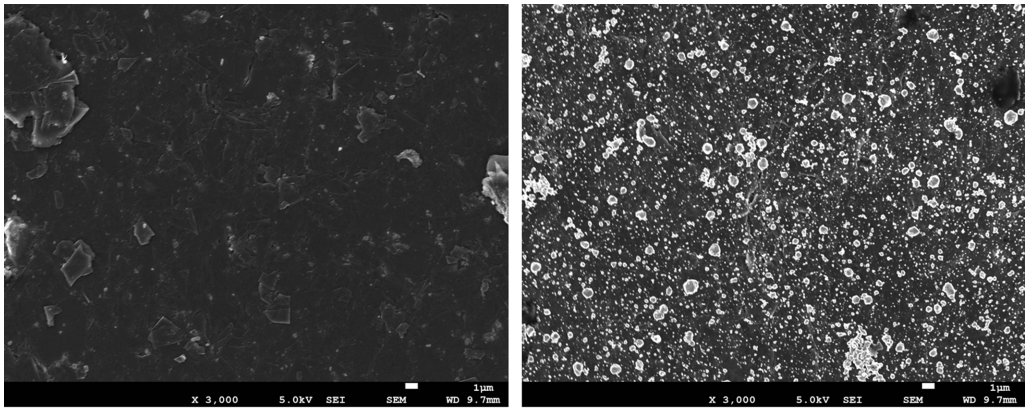

Fig. 4. SEM images of EG (a) and Ag@EG (b) (magnification of 3,000, scale bar of 1 μm).

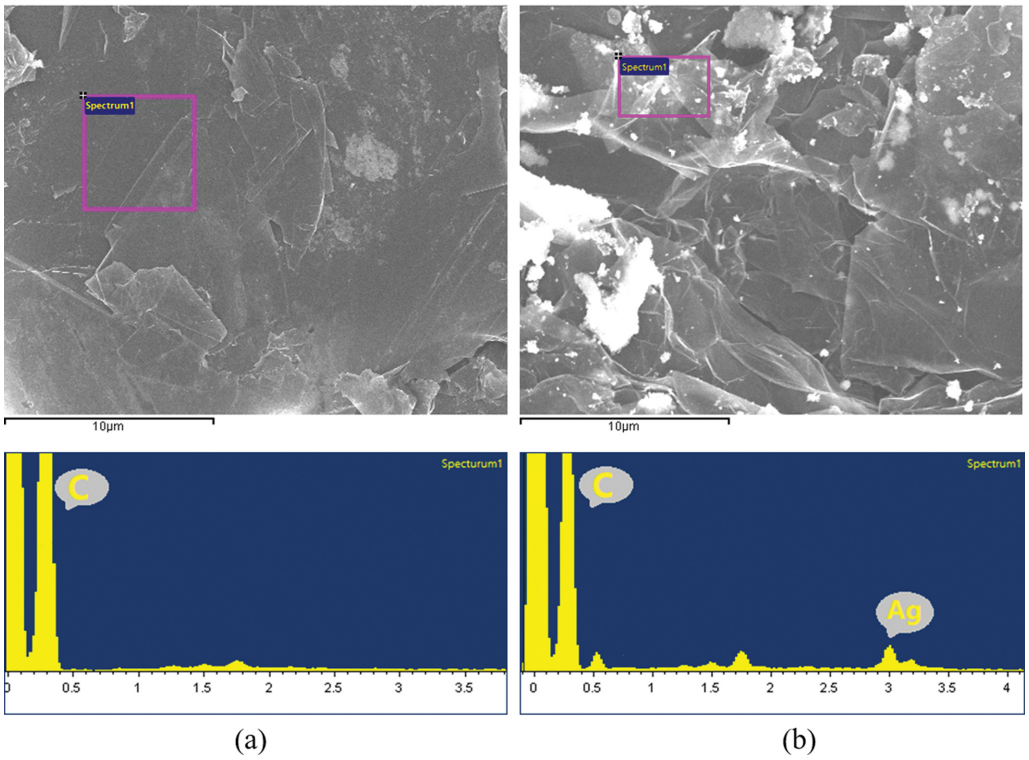

Fig. 5. EDX maps of EG (a) and Ag@EG (b).

RESULTS AND DISCUSSION

1. Characterization of Silver Plating

Fig. 3 shows the FTIR spectra of EG before and after the silver plating. As shown in Fig. 3, the absorption peak at 3,428 cm^{-1} is attributed to the stretching vibration of the hydroxyl group, and the intensity of the hydroxyl peak decreases after the silver plating. This result indicates that the EG surface contains hydroxyl group, which exhibits a certain negative charge. Therefore, the EG surface adsorbs the silver cations from the silver solution, thereby aiding the silver particles to nucleate and grow on the EG surface. When glucose as a reducing agent was added, the silver cations were reduced to silver particles, which firmly anchored onto the EG surface [21]. The related reactions are expressed by the following equations:

$$AgNO_3+NaOH=AgOH\downarrow+NaNO_3 \quad (4)$$

$$AgOH+2NH_3\cdot H_2O=Ag(NH_3)_2OH+2H_2O \quad (5)$$

$$C_6H_{12}O_6+2[Ag(NH_3)_2]OH=C_5H_{11}O_5COONH_4+3NH_3+2Ag\downarrow+H_2O \quad (6)$$

To investigate the morphology of the EG before and after the silver plating and to assess the presence of silver on the EG surface, SEM-EDX observations were carried out. Fig. 4 shows the surface morphology of the pristine EG and Ag@EG. As shown in Fig. 4(a), the pristine EG exhibited a smooth surface. In contrast, in the case of Ag@EG, numerous white silver particles appeared on the EG surface after the silver plating [22], as shown in Fig. 4(b). Fig. 5 shows the EDX maps of the pristine EG and Ag@EG. As shown in Fig. 5(a), the peaks at approximately 0.05 and 0.28 keV can be attributed to carbon. A new peak of silver at approximately 3 keV appeared after the silver plating [23], as shown in Fig. 5(b).

The existence of the silver on the EG surface is further evident from the XPS analysis shown in Fig. 6. In Fig. 6(a), the characteristic peak of C_{1s} appears at 284.6 eV, and the C_{1s} peak intensity decreases after the silver plating. Furthermore, as shown in Fig. 6(b), two new peaks are observed at 368.5 and 374.5 eV, which can be attributed to the $Ag_{3d5/2}$ and $Ag_{3d3/2}$ core-level transitions [24,25], respectively. These results verify the successful silver plating of the EG surface.

2. Thermal Conductivity

Fig. 7 shows the variation in the thermal conductivity of the DGEBA/EG composites as a function of the EG content. As shown in Fig. 7, the pristine DGEBA exhibits a low thermal conductivity of 0.17 W/m·K. In contrast, the thermal conductivity of the composites increases with the increasing EG content up to 40 wt%. At the EG content of 40 wt%, the thermal conductivity of the composites is 3.36 W/m·K, which is 19 times higher than that of the pristine DGEBA. Moreover, the thermal conductivity of the composites significantly increases when the EG content is increased above 40 wt%. Evidently, the thermal conductivity of the composites containing 60 and 80 wt% of EG was 7.35 and 11.27 W/m·K, respectively, which is 42 and 66 times higher than that of the pristine DGEBA. These results indicate that the EG can exhibit a high thermal conductivity of 300 W/m·K [26]. In addition, the EG dispersed in the DGEBA matrix formed a thermal conductive network, which in turn enhanced the thermal conductivity of the DGEBA/EG composites [27].

The effect of silver plating on the thermal conductivity of the

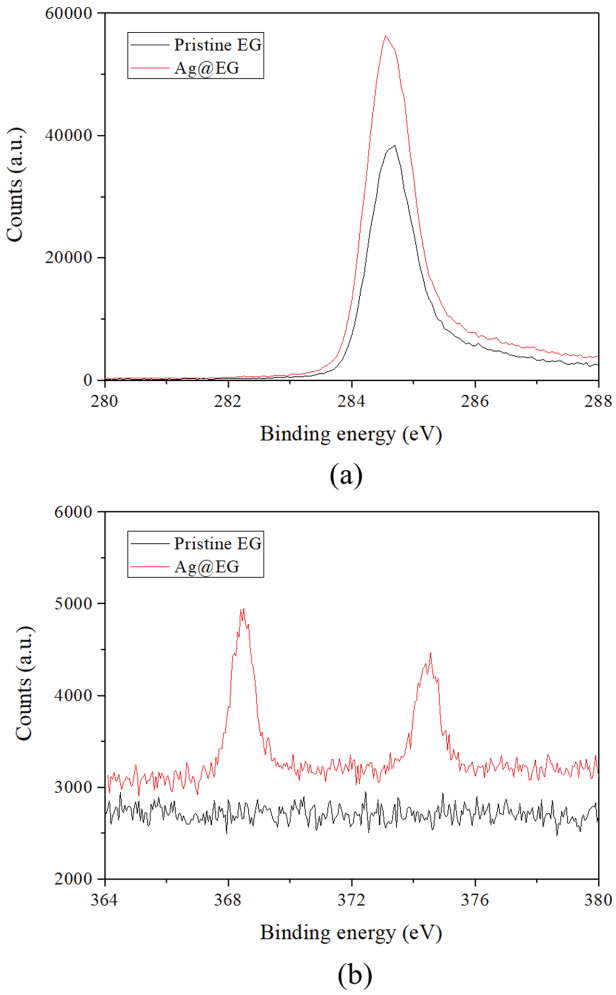

Fig. 6. XPS spectra of EG and Ag@EG: (a) high-resolution C_{1s}, (b) high-resolution Ag_{3d}.

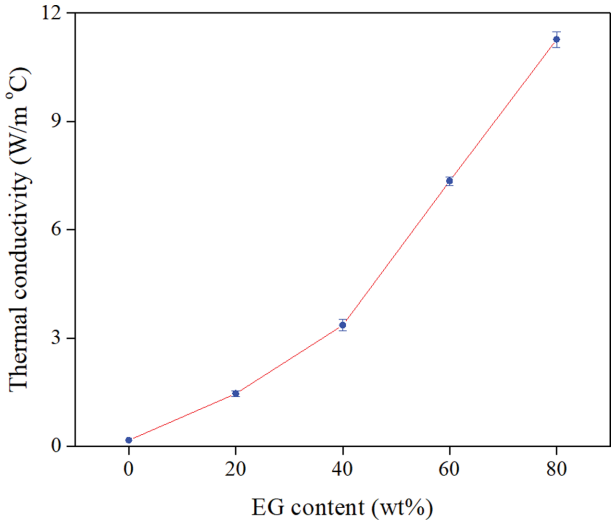

Fig. 7. Thermal conductivity of DGEBA/EG composites as a function of EG content.

Table 1. Thermal and electrical conductivity of DGEBA/EG composites with and without silver plating

EG content (wt%)	Silver plating	Thermal conductivity (W/m·°C)	Electrical conductivity (S/cm)
60	No	7.35	0.62
60	Yes	9.49	0.78

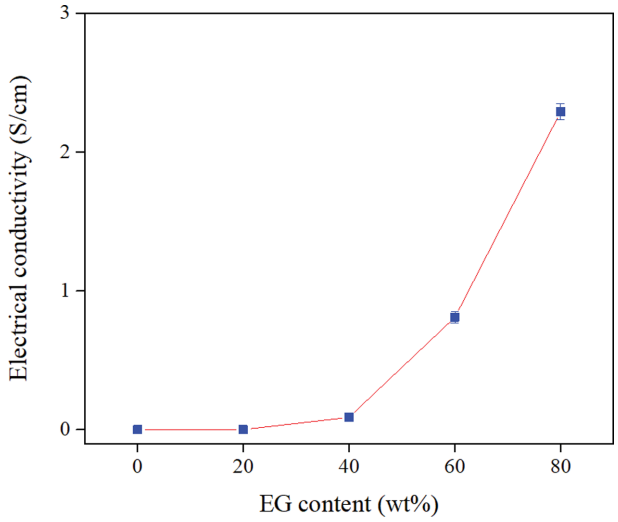

Fig. 8. Electrical conductivity of DGEBA/EG composites as a function of EG content.

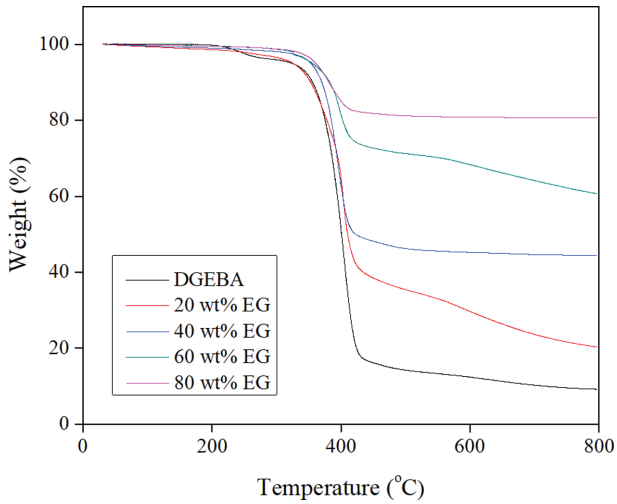

Fig. 9. TGA thermograms of DGEBA/EG composites as a function of EG content.

DGEBA/EG composites was investigated, and the corresponding results are shown in Table 1. Notably, the thermal conductivity of the DGEBA/EG composites containing 60 wt% of EG is 7.35 W/m·K, whereas that of the DGEBA/Ag@EG composites containing 60 wt% Ag@EG is 9.49 W/m·K, which is 29% higher than that of the DGEBA/EG composites. This increase in the thermal conductivity is caused by the plated silver, whose thermal conductivity (429 W/m·K) is higher than that of the EG. In addition, the silver particles in the DGEBA matrix linked the adjacent EG sheets and formed a thermal conductive network through the electron transfer-thermal mechanism coupled with the acoustic phonons. This thermal conductive network resulted in the observed increase in the thermal conductivity of the DGEBA/Ag@EG composites [28].

3. Electrical Properties

The effect of EG content on the electrical conductivity of the DGEBA/EG composites is indicated in Fig. 8. The electrical conductivity of the pristine DGEBA is 0 S/cm, indicating that pristine DGEBA is an insulating material. Conversely, the electrical conductivity of the composites increased from 0 to 8.95×10^{-2} S/cm with the addition of 40 wt% of EG. Also, the electrical conductivity of the composites increased significantly from 8.95×10^{-2} to 2.29 S/cm when the EG content was increased from 40 to 80 wt%. This increase in the electrical conductivity can be attributed to the high electrical conductivity of EG (500 S/cm), which promotes the formation of an electrically conductive network in the DGEBA matrix [29].

Furthermore, the effect of silver plating on the electrical conductivity of the DGEBA/EG composites was investigated, and the corresponding results are summarized in Table 1. The electrical conductivity of the DGEBA/EG composites containing 60 wt% of EG was 0.62 S/cm, whereas that of the DGEBA/Ag@EG composites containing 60 wt% Ag@EG was 0.78 S/cm, which is 26% higher than that of the DGEBA/EG composites. This result can be attributed to the linking of the adjacent EG sheets by the silver particles, which exhibit a high electrical conductivity. This crosslinking formed an

Table 2. Thermal stability factors of DGEBA/EG composites with and without silver plating obtained from TGA thermograms

EG content (wt%)	Silver plating	$T_{5\%}$ (°C)	Char at 800 °C (%)
0	No	324.7	9.2
20	No	328.5	20.4
40	No	353.3	44.4
60	No	355.8	60.7
80	No	361.3	80.6
60	Yes	359.8	69.3

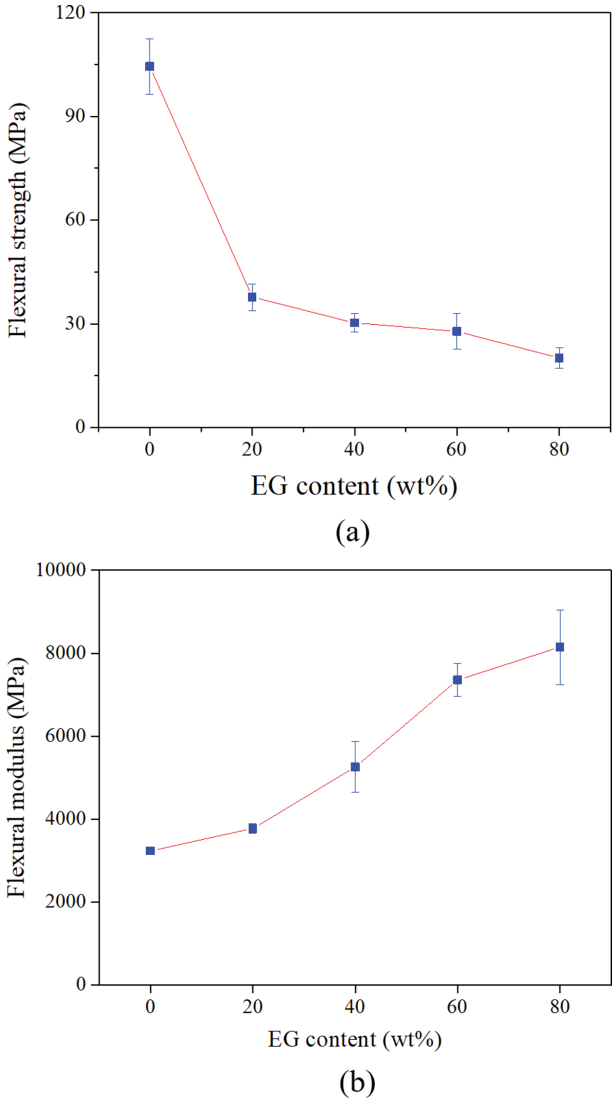

Fig. 10. Flexural strength (a) and flexural modulus (b) of DGEBA/EG composites as a function of EG content.

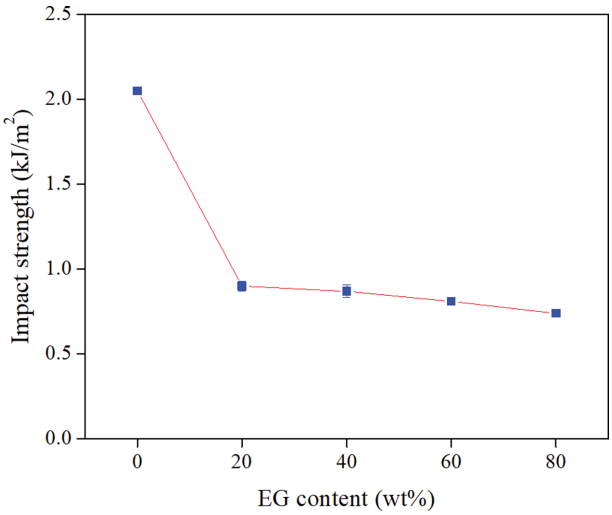

Fig. 11. Impact strength of DGEBA/EG composites as a function of EG content.

electrically conductive network in the DGEBA matrix, thereby increasing the electrical conductivity of the DGEBA/Ag@EG composites [30].

4. Thermal Stability

The effect of EG content on the thermal stability of the DGEBA/EG composites was investigated using TGA. Fig. 9 shows the thermal degradation behavior of the composites as a function of the EG content. Thermal stability factors such as the initial decomposition temperature (i.e., the 5% weight loss temperature ($T_{5\%}$)) and the amount of char formation at 800 °C were calculated from the TGA thermograms [31,32], and the results are summarized in Table 2.

The $T_{5\%}$ value of the composites increased with the addition of EG. That is, the $T_{5\%}$ value of the composites at 60 and 80 wt% of EG is 355.8 and 361.3 °C, respectively, which is 31.1 and 36.6 °C higher than that of the pristine DGEBA. These results can be attributed to the high heat capacity and thermal resistance of the EG than of the pristine DGEBA [33,34]. In addition, the amount of char formation at 800 °C increased from 9.2% to 80.6%, with increasing the EG content from 0 to 80 wt%, because of the large residual mass of EG.

Furthermore, the effect of silver plating on the thermal stability of the DGEBA/EG composites was investigated, and the resulting thermal stability factors are listed in Table 2, which indicates that the thermal stability of the composites increased with the silver plating. In detail, the $T_{5\%}$ value of the DGEBA/Ag@EG composites at 60 wt% Ag@EG is 359.8 °C, which is 4 °C higher than that of the DGEBA/EG composites containing 60 wt% EG. Moreover, the amount of char formation in the composites at 800 °C increased from 60.7% to 69.3% with the silver plating. These results can be attributed to the high heat capacity and large residual mass of silver [34].

5. Flexural Properties

The flexural property of the DGEBA/EG composites was investigated by measuring their flexural strength and moduli. The effect of EG content on the flexural strength of the DGEBA/EG composites is presented in Fig. 10(a). The flexural strength of the composites decreases remarkably from 104.4 MPa at a graphene content of 0 wt% to 37.7 MPa at an EG content of 20 wt%. In addition, the flexural strength of the composites further decreases gradually from 37.7 to 20.2 MPa when the EG content increases from 20 to 80 wt%. These observations can be attributed to the aggregation of

Table 3. Flexural property and impact strength of DGEBA/EG composites with and without silver plating

EG content (wt%)	Silver plating	Flexural strength (MPa)	Flexural modulus (MPa)	Impact strength (kJ/m^2)
60	No	27.9	7,355.7	0.81
60	Yes	28.7	7,608.2	0.80

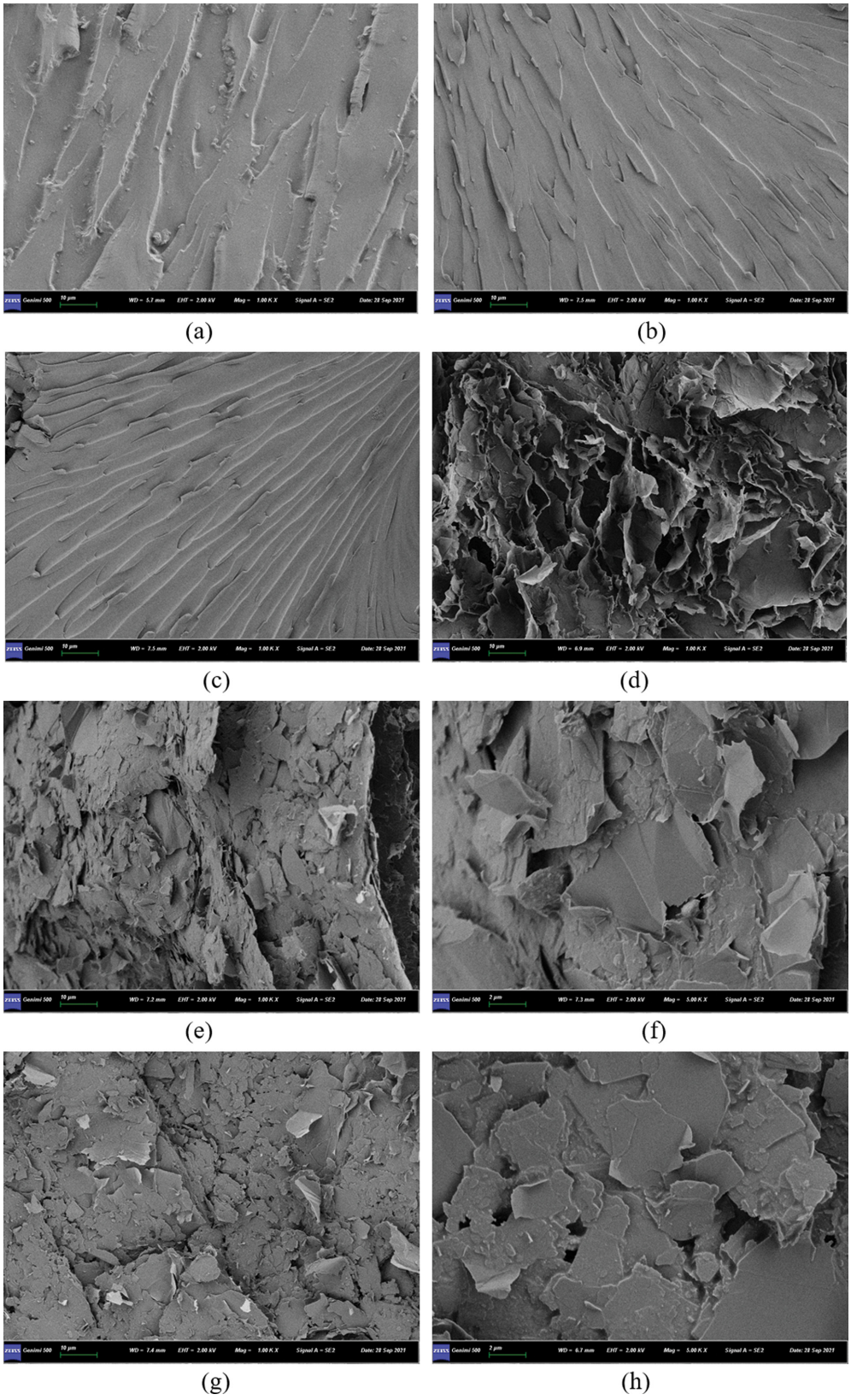

Fig. 12. SEM micrographs of DGEBA/EG and DGEBA/Ag@EG composites: (a) pristine DGEBA (magnification of 1,000, scale bar of 10 μm), (b) 20 wt% EG (magnification of 1,000, scale bar of 10 μm), (c) 40 wt% EG (magnification of 1,000, scale bar of 10 μm), (d) 60 wt% EG (magnification of 1,000, scale bar of 10 μm), (e) 80 wt% EG (magnification of 1,000, scale bar of 10 μm), (f) 80 wt% EG (magnification of 5,000, scale bar of 2 μm), (g) 60 wt% Ag@EG (magnification of 1,000, scale bar of 10 μm), (h) 60 wt% Ag@EG (magnification of 5,000, scale bar of 2 μm).

most of the EG in the DGEBA matrix at high EG content, resulting in the observed decrease in the flexural strength of the DGEBA/EG composites [35].

Fig. 10(b) shows the variation in the flexural modulus of the DGEBA/EG composites with increasing EG content, indicating that the flexural modulus of the composites increased significantly with the addition of EG. The pristine DGEBA exhibits a flexural modulus of 3,234 MPa. In contrast, the flexural modulus of the composites at 80 wt% of EG is 8,146 MPa, which is 151% higher than that of the pristine DGEBA. These results can be attributed to the addition of EG, which increases the stiffness of the composites, and as a result, increases the flexural modulus of the DGEBA/EG composites [36].

Additionally, the effect of silver plating on the flexural property of the DGEBA/EG composites was investigated, and the results of flexural strength and flexural modulus are summarized in Table 3. Evidently, the flexural strength and flexural modulus values of the DGEBA/Ag@EG composites at 60 wt% Ag@EG are 28.7 and 7,608.2 MPa, respectively, which are 2.9% and 3.4% higher than those of the DGEBA/EG composites containing 60 wt% EG. These results indicate that the flexural properties of the DGEBA/EG composites slightly improved with the silver plating.

6. Impact Strength

The effect of EG content on the impact strength of the DGEBA/EG composites is presented in Fig. 11. The impact strength decreases drastically from 2.0 kJ/m^2 at an EG content of 0 wt% to 0.9 kJ/m^2 at an EG content of 20 wt%. In addition, the impact strength of the composites decreases gradually from 0.9 to 0.74 kJ/m^2 when the EG content increases from 20 to 80 wt%. These results can be attributed to the agglomeration of EG and the stress concentration induced by the aggregated EG in the DGEBA matrix at high EG contents, resulting in the observed decrease in the impact strength of the DGEBA/EG composites [35,37].

The effect of silver plating on the impact strength of the DGEBA/EG composites was investigated as well, and the corresponding results are presented in Table 3, revealing that the impact strength value of the DGEBA/Ag@EG composites at 60 wt% Ag@EG is 0.8 kJ/m^2. This value is similar to that of the DGEBA/EG composites containing 60 wt% EG, implying that the silver plating did not affect the impact strength of the DGEBA/EG composites significantly.

7. Morphology

The morphology of the pristine DGEBA, DGEBA/EG composites, and DGEBA/Ag@EG composites after the impact strength tests was investigated using SEM, and the corresponding SEM images of the fractured surfaces are depicted in Fig. 12. The pristine DGEBA shows an ordered cracking morphology, as shown in Fig. 12(a) [38]. For an EG content of 20 wt%, the DGEBA/EG composites exhibit a morphology similar to that of the pristine DGEBA. However, cracks begin to narrow, and the interface between the EG and DGEBA matrix becomes weaker [39], as shown in Fig. 12(b). For an EG content of 40 wt%, the DGEBA/EG composites exhibit a mirror-like morphology with an ordered cracking behavior, as shown in Fig. 12(c). The high-resolution images shown in Fig. 12(d)-(f) reveal that when the EG content is further increased to 60 and 80 wt%, the sheet-shaped blocks peel away from the fractured surfaces under an external force, accounting for its low impact strength [40]. Under this condition, the EG sheets form a continuous local conductive path, thereby enhancing the thermal and electrical conductivities of the DGEBA/EG composites [41]. The DGEBA/Ag@EG composites containing 60 wt% Ag@EG exhibit a morphology of sheet-shaped blocks peeled away from the fractured surfaces, which is similar to that of the DGEBA/EG composites containing 60 and 80 wt% EG, as shown in Fig. 12(g) and 12(h).

CONCLUSIONS

DGEBA/EG composites, with and without silver plating, were prepared via melt blending and compressioncuring processes, and their thermal and electrical conductivity, thermal property, flexural property, impact strength, and morphology were investigated. The results indicated that the thermal conductivity of DGEBA/EG composites increased from 0.17 to 7.35 W/m·K with addition of 60 wt% of EG and further increased to 9.49 W/m·K when the EG surface was silver plated. The electrical conductivity of the DGEBA/EG composites increased from 0 to 0.62 S/cm with the addition of 60 wt% of EG and further increased to 0.78 S/cm after silver plating of the EG surface. The $T_{5\%}$ values of the composites containing 60 and 80 wt% of EG were 31.1 and 36.6 °C higher than that of the pristine DGEBA, respectively. The addition of EG caused two opposite phenomena: a decrease in the flexural strength and a significant increase in the flexural modulus of the composites. The impact strength of the composites decreased with the increasing EG content. The SEM results revealed that the EG sheets in the DGEBA matrix formed a continuous local conductive path at high EG content.

ACKNOWLEDGEMENTS

This work was supported by the Technology Innovation Program (or Industrial Strategic Technology Development Program-Development of technology on materials and components) (20010106, Adhesives with low water permeability and low outgassing) funded By the Ministry of Trade, Industry & Energy (MOTIE, Korea).

REFERENCES

1. S. J. Park and F. L. Jin, *Carbon fibers: Chapter 3. Matrices for carbon fiber composites*, Springer Series in Materials Science, New York London (2015).
2. T. Zheng, H. Xi, Z. Wang, X. Zhang, Y. Wang, Y. Qian, P. Wang, Q. LI, Z. Li, C. Ji and X. Wang, *Polym. Test.*, **91**, 106781 (2020).
3. Y. I. Hsu, L. Huang and H. Uyama, *Polym. Degrad. Stabil.*, **178**, 109213 (2020).
4. M. A. A. Dzul-Cervantes, O. F. Pacheco-Salazar, L. A. Can-Herrera, M. V. Moreno-Chulim, J. I. Cauich-Cupul, P. J. Herrera-Franco and A. Valadez-Gonzalez, *J. Mater. Res. Technol.*, **9**(6), 15739 (2020).
5. X. Liu and Z. Rao, *Comp. Mater. Sci.*, **172**, 109298 (2020).
6. Y. Xian and Z. Kang, *Prog. Org. Coat.*, **140**, 105486 (2019).
7. Z. Qu, K. Wu, W. Meng, B. Nan, Z. Hu, C. Xu, Z. Tan, Q. Zhang, H. Meng and J. Shi, *Chem. Eng. J.*, **397**, 125416 (2020).
8. J. He, H. Wang, Q. Qu, Z. Su, T. Qin and X. Tian, *Compos. Part A-*

Appl. S., **139**, 106062 (2020).
9. R. Wang, C. Xie, B. Gou, H. Xu, S. Luo, J. Zhou and L. Zeng, *Polym. Test.*, **89**, 106574 (2020).
10. J. He, H. Wang, Q. Qu, Z. Su, T. Qin, Y. Da and X. Tian, *Compos. Commun.*, **22**, 100448 (2020).
11. Y. Xian, Z. Kang and Y. He, *Prog. Org. Coat.*, **147**, 105859 (2020).
12. M. Zhu, L. Liu and Z. Wang, *Compos. Part B-Eng.*, **199**, 108283 (2020).
13. C. Xiao, L. Chen, Y. Tang, X. Zhang, K. Zheng and X. Tian, *Compos. Part A-Appl. S.*, **116**, 98 (2019).
14. R. Kumar, S. Mohanty and S. K. Nayak, *Mater. Today Commun.*, **20**, 100561 (2019).
15. X. Ren, H. Shen, Y. Yang and J. Yang, *Phase Transit.*, **92**, 582 (2019).
16. A. Bachar, B. Gurzęda, J. Zembrzuska, M. Nocuń and P. Krawczyk, *J. Solid State Electr.*, **22**, 3965 (2018).
17. Y. Chen, Z. Wang, R. Xu, W. Wang and D. Yu, *Chem. Eng. J.*, **394**, 124960 (2020).
18. O. Güler, T. Varol, Ü. Alver and A. Çanakçı, *J. Alloys Compd.*, **782**, 679 (2019).
19. S. D. Kim, W. Choe, J. Choi and J. R. Jeong, *Powder Technol.*, **342**, 301 (2019).
20. Q. Zhao, M. Xie, Y. Liu and J. Yi, *Appl. Surf. Sci.*, **409**, 164 (2017).
21. L. Ren, Q. Li, J. Lu, X. Zeng, R. Sun, J. Wu, J. B. Xu and C. P. Wong, *Compos. Part A-Appl. S.*, **107**, 561 (2018).
22. Y. Mao, S. Zhang, W. Wang and D. Yu, *Colloid. Surf. A*, **558**, 538 (2018).
23. Y. J. Yim and S. J. Park, *Compos. Part A-Appl. S.*, **123**, 253 (2021).
24. L. P. Wu, Y. Z. Li, B. J. Wang, Z. P. Mao, H. Xu, Y. Zhong, L. P. Zhang and X. F. Sui, *Mater. Design*, **159**, 47 (2018).
25. L. Wang, H. Qiu, C. Liang, P. Song, Y. Han, Y. Han, J. Gu, J. Kong, D. Pan and Z. Guo, *Carbon*, **141**, 506 (2019).
26. B. Wei, L. Zhang and S. Yang, *Chem. Eng. J.*, **404**, 126437 (2021).
27. Q. B. Ho, O. Osazuwa, R. Modler, M. Daymond, M. T. Gallerneault and M. Kontopoulou, *Compos. Sci. Technol.*, **176**, 111 (2019).
28. L. Ren, Q. Li, J. Lu, X. Zeng, R. Sun, J. Wu, J. B. Xu and C. P. Wong, *Compos. Part A-Appl. S.*, **107**, 561 (2018).
29. S. Paszkiewicz, A. Szymczyk, X. M. Sui, H. D. Wsilverner, A. Linares, A. Cirera, A. Varea, T. A. Ezquerra and Z. Rosłaniec, *J. Appl. Polym. Sci.*, **134**, 44370 (2017).
30. Y. Zhang, S. Qi, X. Wu and G. Duan, *Synthetic Met.*, **161**, 516 (2011).
31. F. L. Jin, C. L. Ma, B. T. Guo and S. J. Park, *Bull. Korean Chem. Soc.*, **40**(10), 991 (2019).
32. F. L. Jin, H. Zhang, S. S. Yao and S. J. Park, *Macromol. Res.*, **26**(3), 211 (2018).
33. F. Xie, S. H. Qi and D. Wu, *Polym. Compos.*, **38**, 2822 (2015).
34. W. Lin, X. Xi and C. Yu, *Synthetic Met.*, **159**, 619 (2009).
35. H. Wang, S. S. Yao, Z. Guan, F. L. Jin and S.-J. Park, *Korean J. Chem. Eng.*, **38**(11), 2332 (2021).
36. M. Barczewski, O. Mysiukiewicz, D. Matykiewicz, A. Kloziński, J. Andrzejewski and A. Piasecki, *Polym. Test.*, **89**, 106628 (2020).
37. A. K. Singh, Siddhartha and S. Yadav, *Polym. Adv. Technol.*, **28**, 1764 (2017).
38. S. S. Yao, C. L. Ma, F. L. Jin and S. J. Park, *Korean J. Chem. Eng.*, **37**(11), 2075 (2020).
39. Z. Chen, Y. Xu, Y. Yu, T. Chen, Q. Zhang, C. Li and J. Jiang, *Powder Technol.*, **378**, 359 (2021).
40. F. L. Jin, R. R. Hu and S. J. Park, *Korean J. Chem. Eng.*, **37**(5), 905 (2020).
41. I. Isarn, L. Bonnaud, L. Masssilverués, À. Serra and F. Ferrando, *Prog. Org. Coat.*, **133**, 299 (2019).